Molecular Imaging Hot Paper

Deutsche Ausgabe: DOI: 10.1002/ange.201607751
Internationale Ausgabe: DOI: 10.1002/anie.201607751

Molecular Imaging of Growth, Metabolism, and Antibiotic Inhibition in Bacterial Colonies by Laser Ablation Electrospray Ionization Mass Spectrometry

*Hang Li, Pranav Balan, and Akos Vertes**

Abstract: *Metabolism in microbial colonies responds to competing species, rapidly evolving genetic makeup, and sometimes dramatic environmental changes. Conventional characterization of the existing and emerging microbial strains and their interactions with antimicrobial agents, e.g., the Kirby–Bauer susceptibility test, relies on time consuming methods with limited ability to discern the molecular mechanism and the minimum inhibitory concentration. Assessing the metabolic adaptation of microbial colonies requires their non-targeted molecular imaging in a native environment. Laser ablation electrospray ionization (LAESI) is an ambient ionization technique that in combination with mass spectrometry (MS) enables the analysis and imaging of numerous metabolites and lipids. In this contribution, we report on the application of LAESI-MS imaging to gain deeper molecular insight into microbe–antibiotic interactions, and enhance the quantitative nature of antibiotic susceptibility testing while significantly reducing the required incubation time.*

With the emergence of multidrug resistant microbial strains and bacterial pathogens, the need for rapid and accurate testing of antibiotic susceptibility is increasing.[1–3] Understanding microbial metabolism and its inhibition by the antibiotic is important for developing new treatments of bacterial infections.

Conventional antibiotic susceptibility testing (e.g., the Kirby–Bauer (KB) method) has been widely used for determining drug resistance in clinical microbiology.[4] However, these techniques require a relatively long incubation time of 16–24 h and lack the capability of determining the minimum inhibitory concentration (MIC). Their efficacy is limited for polypeptide antibiotics, anaerobic, slow growing or fastidious bacteria.[5] More recent commercialized versions of the KB approach, e.g., M.I.C.Evaluator and Etest, provide MIC values for different microbial colonies based on test strips with built-in antibiotics gradients.[6]

[*] Dr. H. Li, Prof. A. Vertes
Department of Chemistry, The George Washington University
Washington, DC 20052 (USA)
E-mail: vertes@gwu.edu
Homepage: http://vertes.columbian.gwu.edu
P. Balan
Thomas Jefferson High School for Science and Technology
Alexandria, VA 22312 (USA)
Supporting information and the ORCID identification number(s) for the author(s) of this article can be found under http://dx.doi.org/10.1002/anie.201607751.

Emerging antimicrobial susceptibility testing techniques, including microarrays, whole-genome sequencing, and polymerase chain reaction-based approaches, have all shown promise but it remains to be determined if they possess sufficient sensitivity and specificity.[7,8] Mass spectrometry (MS) was also introduced for studying the resistance of bacteria to various antimicrobial agents. With matrix-assisted laser desorption ionization (MALDI) time-of-flight (TOF) MS, susceptible and resistant isolates of selected microbial model systems, such as *Escherichia coli*, *Staphylococcus aureus*, *Pseudomonas aeruginosa*, were distinguished based on mass spectral features obtained from whole cell pellets or extracts.[8]

In addition, MS and MS imaging (MSI) have played an important role in characterizing the microbial metabolism and investigating the interactions between different phenotypes of bacteria.[9] Secondary ion MS (SIMS)[10] and MALDI-MS,[11,12] as the ionization source under vacuum condition, allowed for high resolution imaging of biomolecular distributions in bacterial communities or interacting microbial colonies. Laser desorption postionization (LDPI) MS with vacuum ultraviolet single photon ionization also enabled the imaging and depth profiling of bacterial biofilms.[13,14] Ambient ionization based MS techniques, such as desorption electrospray ionization (DESI),[15] nano-DESI,[16,17] paper spray,[18] and swab touch spray ionization,[19,20] have been recently developed for imaging and rapid metabolic analysis of microbes in their native environment.

Laser ablation electrospray ionization (LAESI)-MS, an ambient ionization technique, is a tool for the detection, imaging, and depth profiling of metabolites in biological cells and tissues. Both two-dimensional (2D) and three-dimensional (3D) imaging was demonstrated for animal and plant tissues.[21,22] The distribution of a large variety of metabolites and lipids were mapped on tissue sections and meaningful correlations with biological functions were observed. Recently, integrating ion mobility separation (IMS) with LAESI-MS or LAESI-MSI facilitated the separation of isobaric ions based on their drift time (DT) and resulted in enhanced metabolite coverage.[23,24]

In this contribution, LAESI-IMS-MS and LAESI-MSI were utilized to characterize the distributions of a wide array of metabolites and lipids in *E. coli* (ATCC 12435) and *B. subtilis* (ATCC 6051) model microorganisms interacting with antibiotics in Kirby–Bauer type experiments. Antibiotic inhibition of bacterial growth was investigated using 2D and 3D molecular imaging. Experimental methods and mathematical modeling to probe the antibiotic diffusion process are described in the Supporting Information (SI).

Plotting the ion intensities as a function of DT and *m/z* for *B. subtilis* colonies (see Figure S1 in the SI) illustrated the diverse biomolecules detected by LAESI-IMS-MS. Metabolites, lipids, and multiply charged peptides were separated in different regions of the DT vs. *m/z* plot marked by green ovals. Negative (Figure S1a) and positive ion mode (Figure S1b) results complemented each other, enabling the detection of, e.g., nucleoside phosphates and amino acids, respectively. By combining these two modes, over 400 deisotoped spectral features have been detected. To identify the detected ions, accurate *m/z* measurements, tandem MS, collision cross section (CCS) determination, and database searches were jointly employed. To characterize the quality of identification we adopted the four level scheme introduced by the Metabolomics Standards Initiative.[25] Details of the ion identification process and the quality of identification are described in the SI. Based on these results, lists of identified 24 metabolites (Table S1), 40 lipids (Table S2), and 2 peptides were generated for *B. subtilis* and *E. coli*.

Some of the identified molecules belonged to important metabolic pathways, including purine degradation, and the metabolism of pyrimidine, alanine, glutathione, and glycerophospholipids. Comparing the identified ions in the Gram-positive *B. subtilis* and the Gram-negative *E. coli*, a significant overlap was observed in their metabolites and lipids. Certain molecules, for example surfactin, a cyclic lipopeptide, found only in *B. subtilis*, can serve as biomarkers.

To explore the distribution of endogenous metabolites and lipids within a colony, we performed three-dimensional (3D) LAESI-MSI. Figure 1a shows the optical images of a colony, an ablation crater with ca. 150 μm diameter, and the cross sectional view of a colony with an ablation mark. The thickness of an isolated *E. coli* colony was between 80 to 100 μm. With a single laser pulse (0.9 mJ/pulse) producing a ca. 25 μm deep crater, crude depth profiling can be achieved by acquiring individual spectra from three to four consecutive laser pulses. Collecting depth profiles for every probed position on the surface enabled the construction of 3D molecular images. For example, in Figure 1b the 3D distributions of acetylspermidine at *m/z* 188.177, and PE(16:0/17:1) at *m/z* 704.523 exhibited decreasing intensities in deeper layers with the former retaining a stronger signal on the perimeter (see Figure S2a and c in the SI for identification). As a control, a prominent peak from the agar medium at *m/z* 758.409 showed similar intensities and distributions in different layers, indicating consistent signal regardless of depth.

The ability to determine the distributions of metabolites and xenobiotics enables us to investigate the antibiotic susceptibility of bacterial growth using LAESI-MSI in combination with KB type experiments. An inoculated *B. subtilis* culture plate was treated with a penicillin–streptomycin paper disc. After 18 h of incubation, a zone of inhibition (ZOI) with a diameter of 21 mm was observed (Figure 2a).

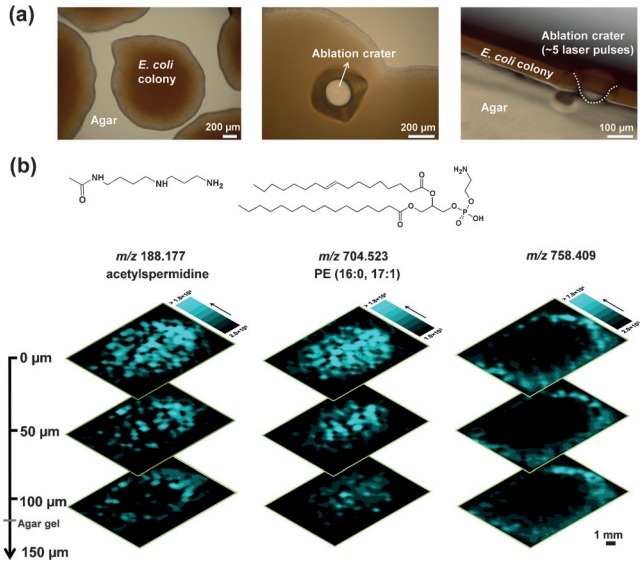

Figure 1. a) Microscope images of *E. coli* colonies. Three images from left to right show a single colony surrounded by neighboring ones, top view of an ablation crater with a diameter of 150 μm, and the side-view indicating the thickness of the colony as 80–100 μm. The side view image also shows the cross sectional view of an ablation crater resulting from five laser pulses. b) Three-dimensional molecular distributions of (left) acetylspermidine at *m/z* 188.177, (middle) PE(16:0/17:1) at *m/z* 704.523, and (right) a prominent peak from the agar medium at *m/z* 758.409.

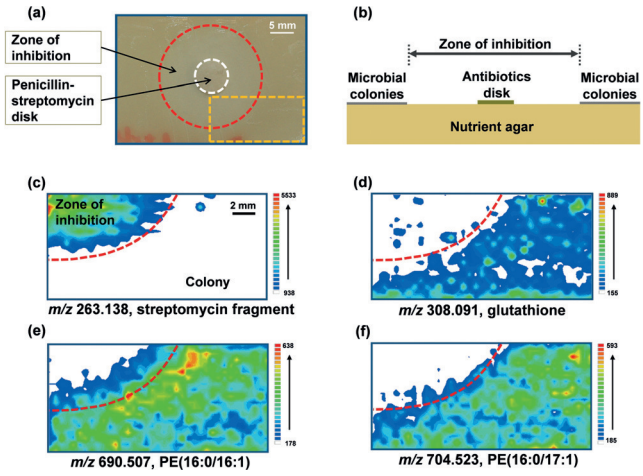

Figure 2. Molecular imaging of antibiotics inhibition on *B. subtilis* colonies. a) *B. subtilis* agar plate after the KB susceptibility testing indicates the produced ZOI (red circle), the penicillin–streptomycin disc (white circle), and the imaged interface region (orange rectangle). b) A side-view schematic of the agar plate reveals the depth dimension, and the antibiotics disc was removed prior to LAESI-MSI. Molecular distribution images of (c) streptomycin fragment at *m/z* 263.138, d) glutathione at *m/z* 308.091, e) PE(16:0/16:1) at *m/z* 690.507, and f) PE(16:0/17:1) at *m/z* 704.523 illustrate the inhibition of *B. subtilis* colonies by the diffusion of streptomycin.

Figure 2b illustrates the cross sectional view showing the antibiotic infused paper disc and the bacterial colonies on top of the agar. The disc was removed prior to the imaging experiment and part of the interface between the ZOI and the colony was imaged (see orange rectangle in Figure 2a). As shown in Figure 2c, the abundance of streptomycin fragment with *m/z* 263.138 was high at the location where the disc has been placed then it decreased towards the edge of the ZOI,

and eventually it was obscured by the bacterial colony. In contrast in Figure 2 d, e and f, the glutathione at *m/z* 308.091 (see Figure S2b in the SI for identification) and the two phosphatidylethanolamine (PE) ions at *m/z* 690.507 and 704.523, respectively, were abundant in the colony but absent in the ZOI. Interestingly, the PE(16:0/16:1) lipid showed increased levels toward the edge of the colony and it was even present in part of the ZOI, whereas, glutathione and PE(16:0/17:1) were not present in the ZOI.

The constructed 3D images (Figure 3) showed the distribution of molecules at three layers of increasing depths of 50 μm each. As the thickness of the colony is ca. 100 μm, the ions detected at depths between 100 and 150 μm included signal from the underlying agar medium. The images of a streptomycin fragment distribution in Figure 3 a reflected both radial and depthwise diffusion away from the disc.

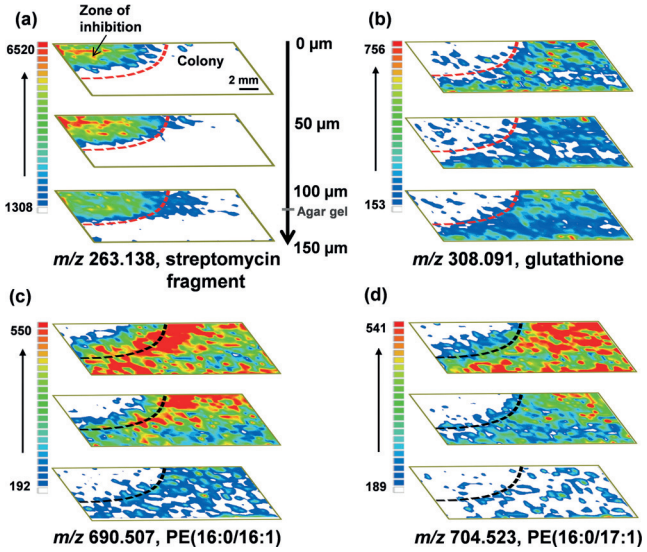

Figure 3. Three-dimensional distributions of a) streptomycin fragment at *m/z* 263.138, b) glutathione at *m/z* 308.091, c) PE(16:0/16:1) at *m/z* 690.507, and d) PE(16:0/17:1) at *m/z* 704.523 in KB susceptibility testing for *B. subtilis*. Streptomycin diffuses both radially and depthwise into the agar. Glutathione exhibits similar distributions in the three layers of increasing depths, whereas lipids PE(16:0/16:1) and PE(16:0/17:1) show a significantly lower abundance in the bottom layer.

(*B. subtilis*) in the presence of streptomycin by LAESI-MSI enabled us to determine if the presence of the antibiotic induced elevated levels of glutathione. Observing the related distribution in Figure 3 b, there seems to be no increase in the glutathione intensities close to the zone of inhibition where the streptomycin concentrations are higher.

As different species of bacteria can coexist in an environment, it is interesting to explore their differential inhibition by antibiotics. Two halves of an agar plate were inoculated with *B. subtilis* and *E. coli*, respectively (see inset in Figure 4), and

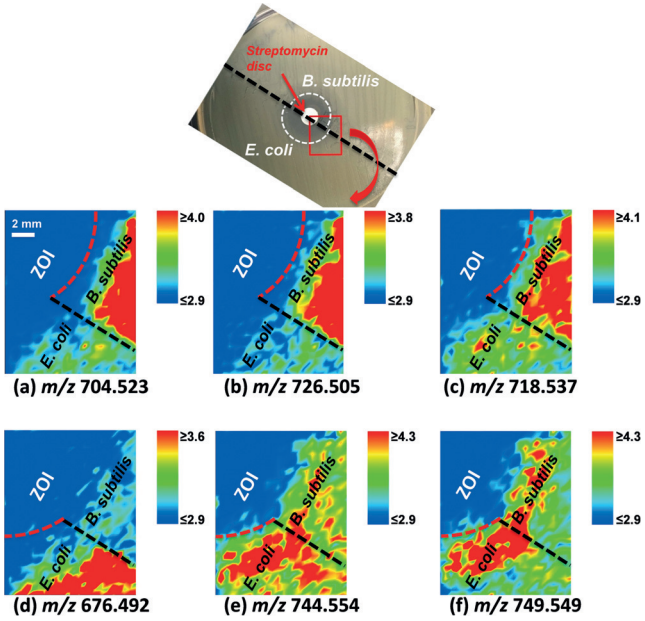

Figure 4. Molecular imaging of antibiotics inhibition on adjacent bacterial colonies separated by black dashed line. The inset shows an agar plate with the top half inoculated with *B. subtilis* and the bottom half with *E. coli*. An antibiotics susceptibility test was performed on the plate with 40 μg streptomycin disc placed in the center. The highlighted red rectangular region corresponds to the imaged area, and molecular distribution images of a) PE(16:0/17:1), $[M+H]^+$, b) PE(16:0/17:1), $[M+Na]^+$, c) PE(16:0/18:1), $[M+H]^+$, d) PE(31:1), $[M+H]^+$, e) PE(18:1/18:1), $[M+H]^+$, and f) PG(34:1), $[M+H]^+$ are displayed. Boundary of ZOI is shown by red dashed line. The label of the false color scale bar is the logarithm of the ion intensity.

Interestingly, streptomycin fragment was detected in the deepest layer even under the colonies, indicating that in these regions the levels of the antibiotic in the agar were below the MIC. Glutathione exhibited distributions that were similar at different depths with slightly higher abundances in the top layer, whereas PE(16:0/17:1) and PE(16:0/16:1) both exhibited a significantly weaker signal from the bottom layer. A possible explanation of relatively high glutathione intensities from the bottom layer was the leakage of this compound from the bacteria followed by diffusion into the top layers of the agar.

Recent investigations of its impact on the susceptibility of some bacteria (*E. coli*) toward streptomycin revealed that glutathione reduced the effectiveness of the antibiotic.[26] Imaging the distribution of glutathione produced by bacteria a streptomycin disc was placed in the center. After 21 h of incubation, molecular distributions of different lipids exhibited distinct features. For example, PE(16:0/17:1) (in protonated and sodiated form), and PE(16:0/18:1) showed significantly higher abundances for the regions inhabited by *B. subtilis* colonies (see Figure 4 a–c), whereas PE(31:1), PE(18:1/18:1), and PG(34:1) were more prevalent in the areas covered by *E. coli* (see Figure 4 d–f). These findings indicate which lipids can be utilized to distinguish between the *B. subtilis* and *E. coli* colonies. To verify that the two optical zone diameters (ZDs) measured in the system with the adjacent colonies of *E. coli* and *B. subtilis* reflect their individual ZDs, we performed the KB susceptibility test on two plates with *E. coli* and *B. subtilis* separately. The observed ZDs for *E. coli* and *B. subtilis* on the single species plates (see

Figure S8a and c) were the same as the values determined on the single plate that contained the two colonies adjacent to each other (see Figure S8b in the SI).

Using density profiles derived from optical imaging, a difference was observed between the ZOIs with diameter values of 15.6 mm and 18.0 mm for *B. subtilis* and *E. coli*, respectively. The spatial distributions for the ion with nominaL *m*/*z* 719 and 750, reporting on *B. subtilis* and *E. coli*, respectively, determined by LAESI-MSI (see panels c and f in Figure 4) indicated zone diameter (ZD) values of $ZD_{719} = 14.5$ mm and $ZD_{750} = 17.8$ mm, respectively. These results are in good agreement with the optically observed values and indicate reduced susceptibility to streptomycin for *B. subtilis* compared to *E. coli*.

In contrast to ZD_{719} for *B. subtilis* and ZD_{750} for *E. coli* that were close to the optically observed ZD values, the distributions for PE(16:0/17:1) and PE(31:1) in these cultures (see Figure 4a and d) indicated that the ZD_{705} and ZD_{676} for those two lipids were significantly larger than the optically determined ZDs. The dissimilar ZD values for different lipids for a given microorganism indicated that certain biochemical pathways were more efficiently inhibited by the antibiotic. This new insight is provided by the combination of LAESI-MSI and the KB test.

The diffusion of antibiotics in agar was examined using a one-dimensional mathematical model and compared with the experimental data from LAESI-MS. Based on the profiling data for *E. coli* colonies at 21 h (75600 s) of incubation, the detected streptomycin ion intensity profile was fitted using the one-dimensional diffusion model (see Figure S5), whereas the ion abundance profile of PG(34:1) from *E. coli* was fitted using a Gaussian curve to reflect a maximum close to the zone of inhibition. The diffusion coefficient of streptomycin in the agar at 37 °C, $D = 1.3 \times 10^{-6}\,cm^2 s^{-1}$, was determined by fitting the diffusion model to the experimental streptomycin profile. As the intensity of streptomycin signal decreased at the edge of the ZOI, the PG(34:1) signal increased, indicating the growing population of bacteria. The critical concentration (c_{cr}) corresponding to the MIC of streptomycin for *E. coli* was determined as the antibiotic concentration at the position with 50% of the microorganisms inhibited, corresponding to $ZD_{750} = 17.8$ mm in Figure S5. The distribution of this ion closely mirrored the optical density profile of the bacterial colonies. At 21 h of incubation, the streptomycin concentration under the center of the disk was estimated to be 1341 $\mu g\,mL^{-1}$ according to the one-dimensional model described in the SI. The c_{cr} for *E. coli* was determined by comparing the streptomycin concentrations at $x = 8.9$ mm with that at the origin ($x = 0$). The c_{cr} of streptomycin determined for *E. coli* was 240 $\mu g\,mL^{-1}$, which fell in the MIC range reported by the European Committee on Antimicrobial Susceptibility Testing (EUCAST) (the database at http://mic.eucast.org/Eucast2/ was last accessed on January 28, 2016). Alternatively, the c_{cr} of streptomycin for *E. coli* can be calculated based on the Vesterdal model.[27,28] Based on Figure S6 in the SI, a value of 180 $\mu g\,mL^{-1}$ was obtained, which was consistent with our result above. To explore the potential of LAESI-MS for faster assessment of antibiotic susceptibility, we profiled the ion abundance distributions of streptomycin and PE(16:0/16:1) from *E. coli* after 5 h of incubation, a considerably shorter period than the typical 16 to 24 h required for the conventional KB test. The generated results are shown in Figure S9 in the SI. Applying the one-dimensional diffusion model and a sigmoidal growth curve (double Boltzmann) to the streptomycin and PE(16:0/16:1) distributions, respectively, the MIC value was estimated to be 285 $\mu g\,mL^{-1}$ (see Figure S9). This result was consistent with the MIC value obtained at 21 h incubation time (240 $\mu g\,mL^{-1}$), and with the database values.

In conclusion, 2D and 3D molecular imaging by LAESI-MSI of microbial cultures and the inhibition of their growth by antibiotics enriched the concept of the ZOI by distinguishing between the optically detected and molecular distributions. The revealed chemical information has the potential to enhance antibiotic susceptibility testing. A method combining mathematical modeling with LAESI-MS profiling was demonstrated for determining the MIC value after a significantly shorter incubation period. Further, these results indicate the potential of LAESI-MSI to study antibiotic diffusion patterns in tissues qualitatively and quantitatively, and to explore complex bacterial interactions.

Acknowledgements

This material is based upon work supported by the U.S. Department of Energy, Office of Science, Office of Basic Energy Sciences, Chemical Sciences, Geosciences and Biosciences Division under Award Number DE-FG02-01ER15129.

Keywords: antibiotic susceptibility · bacteria · laser ablation electrospray ionization · mass spectrometry · molecular imaging

How to cite: *Angew. Chem. Int. Ed.* **2016**, *55*, 15035–15039
Angew. Chem. **2016**, *128*, 15259–15263

[1] M. A. Fischbach, C. T. Walsh, *Science* **2009**, *325*, 1089–1093.
[2] S. E. Dorman, R. E. Chaisson, *Nat. Med.* **2007**, *13*, 295–298.
[3] T. J. Welch, W. F. Fricke, P. F. McDermott, D. G. White, M.-L. Rosso, D. A. Rasko, M. K. Mammel, M. Eppinger, M. J. Rosovitz, D. Wagner, L. Rahalison, J. E. LeClerc, J. M. Hinshaw, L. E. Lindler, T. A. Cebula, E. Carniel, J. Ravel, *Plos One* **2007**, *2*, e309.
[4] J. H. Jorgensen, M. J. Ferraro, *Clin. Infect. Dis.* **2009**, *49*, 1749–1755.
[5] M. K. Cowan, P. K. Talaro, *Microbiology: A Systems Approach*, McGraw-Hill Higher Education, **2009**.
[6] S. Mushtaq, M. Warner, J. Cloke, M. Afzal-Shah, D. M. Livermore, *J. Antimicrob. Chemother.* **2010**, *65*, 1702–1711.
[7] A. Vertes, V. Hitchins, K. S. Phillips, *Anal. Chem.* **2012**, *84*, 3858–3866.
[8] M. R. Pulido, M. Garcia-Quintanilla, R. Martin-Pena, J. M. Cisneros, M. J. McConnell, *J. Antimicrob. Chemother.* **2013**, *68*, 2710–2717.
[9] J. D. Watrous, P. C. Dorrestein, *Nat. Rev. Microbiol.* **2011**, *9*, 683–694.
[10] D. Debois, K. Hamze, V. Guerineau, J.-P. Le Caer, I. B. Holland, P. Lopes, J. Ouazzani, S. J. Seror, A. Brunelle, O. Laprevote, *Proteomics* **2008**, *8*, 3682–3691.

[11] Y.-L. Yang, Y. Xu, R. D. Kersten, W.-T. Liu, M. J. Meehan, B. S. Moore, N. Bandeira, P. C. Dorrestein, *Angew. Chem. Int. Ed.* **2011**, *50*, 5839 – 5842; *Angew. Chem.* **2011**, *123*, 5961 – 5964.
[12] J. Y. Yang, V. V. Phelan, R. Simkovsky, J. D. Watrous, R. M. Trial, T. C. Fleming, R. Wenter, B. S. Moore, S. S. Golden, K. Pogliano, P. C. Dorrestein, *J. Bacteriol.* **2012**, *194*, 6023 – 6028.
[13] A. Akhmetov, J. F. Moore, G. L. Gasper, P. J. Koin, L. Hanley, *J. Mass Spectrom.* **2010**, *45*, 137 – 145.
[14] C. Bhardwaj, J. F. Moore, Y. Cui, G. L. Gasper, H. C. Bernstein, R. P. Carlson, L. Hanley, *Anal. Bioanal. Chem.* **2013**, *405*, 6969 – 6977.
[15] C. F. F. Angolini, P. H. Vendramini, F. D. S. Araújo, W. L. Araújo, R. Augusti, M. N. Eberlin, L. G. de Oliveira, *Anal. Chem.* **2015**, *87*, 6925 – 6930.
[16] J. Watrous, P. Roach, B. Heath, T. Alexandrov, J. Laskin, P. C. Dorrestein, *Anal. Chem.* **2013**, *85*, 10385 – 10391.
[17] J. Watrous, P. Roach, T. Alexandrov, B. S. Heath, J. Y. Yang, R. D. Kersten, M. van der Voort, K. Pogliano, H. Gross, J. M. Raaijmakers, B. S. Moore, J. Laskin, N. Bandeira, P. C. Dorrestein, *Proc. Natl. Acad. Sci. USA* **2012**, *109*, E1743 – E1752.
[18] A. M. Hamid, A. K. Jarmusch, V. Pirro, D. H. Pincus, B. G. Clay, G. Gervasi, R. G. Cooks, *Anal. Chem.* **2014**, *86*, 7500 – 7507.
[19] A. K. Jarmusch, V. Pirro, K. S. Kerian, R. G. Cooks, *Analyst* **2014**, *139*, 4785 – 4789.
[20] V. Pirro, A. K. Jarmusch, M. Vincenti, R. G. Cooks, *Anal. Chim. Acta* **2015**, *861*, 47 – 54.
[21] P. Nemes, A. A. Barton, A. Vertes, *Anal. Chem.* **2009**, *81*, 6668 – 6675.
[22] P. Nemes, A. S. Woods, A. Vertes, *Anal. Chem.* **2010**, *82*, 982 – 988.
[23] B. Shrestha, A. Vertes, *Anal. Chem.* **2014**, *86*, 4308 – 4315.
[24] H. Li, B. K. Smith, L. Márk, P. Nemes, J. Nazarian, A. Vertes, *Int. J. Mass Spectrom.* **2015**, *377*, 681 – 689.
[25] L. W. Sumner, A. Amberg, D. Barrett, M. H. Beale, R. Beger, C. A. Daykin, T. W. M. Fan, O. Fiehn, R. Goodacre, J. L. Griffin, T. Hankemeier, N. Hardy, J. Harnly, R. Higashi, J. Kopka, A. N. Lane, J. C. Lindon, P. Marriott, A. W. Nicholls, M. D. Reily, J. J. Thaden, M. R. Viant, *Metabolomics* **2007**, *3*, 211 – 221.
[26] M. Goswami, S. H. Mangoli, N. Jawali, *Antimicrob. Agents Chemother.* **2007**, *51*, 1119 – 1122.
[27] D. A. Mitchison, C. C. Spicer, *J. Gen. Microbiol.* **1949**, *3*, 184 – 203.
[28] J. W. Mellor, *Higher Mathematics for Students of Chemistry and Physics*, Longmans, Green and co., London, **1902**.

Received: August 10, 2016
Published online: October 4, 2016

